

Multiband Asymmetric Transmission of Airborne Sound by Coded Metasurfaces

Boyang Xie,¹ Hua Cheng,^{1,*} Kun Tang,² Zhengyou Liu,² Shuqi Chen,^{1,†} and Jianguo Tian¹

¹The MOE Key Laboratory of Weak Light Nonlinear Photonics, School of Physics, TEDA Institute of Applied Physics, and the 2011 Project Collaborative Innovation Center for Biological Therapy, Nankai University, Tianjin 300071, China

²School of Physics and Technology and Institute for Advanced Studies, Wuhan University, Wuhan 430072, China

(Received 27 October 2016; published 9 February 2017)

We present the design, characterization, and theoretical and experimental demonstration of multiband asymmetric transmission of airborne sound using an ultrathin coded metasurface formed by an alternating arrangement of the coding elements 0 and 1. The asymmetric transmission effect can be easily controlled to selectively achieve *off* and *on* by coding different patterns. Both frequency- and angle-selective transmission is discussed. The proposed multiband asymmetric transmission stems from the constructive and destructive interferences of acoustic-wave coupling between the coded elements. The experimental results are in relative agreement with numerical simulations. This work opens an alternative path for ultrathin acoustic-device design and shows promise for application in acoustic rectification and noise control.

DOI: 10.1103/PhysRevApplied.7.024010

I. INTRODUCTION

Electrical diodes have revolutionized the development of information technology. Asymmetric transmission, which manifests itself as a difference in the total transmission between forward and backward propagation, has long been an active field of study in information processing because of its utility in constructing electromagnetic and acoustic devices. Asymmetric transmission has been demonstrated in metamaterial designs for both photonics and acoustics. Compared to materials with bulky band-gap structures, metamaterials offer extraordinary advantages in efficiency and integration. Metamaterials with thickness in the sub-wavelength scale can significantly modulate waves because of strong internal local resonance [1]. By breaking the symmetry of unit design, optical metamaterials in particular use polarization-convert elements and chiral structure to achieve asymmetry [2,3]. By contrast, acoustic diodes use scattering [4–6], nonlinear materials [7–9], thermodynamics [10] and index-near-zero metamaterials to generate asymmetry [11–13].

Very recently, topological acoustic metamaterials have been shown to exhibit nonreciprocal one-way edge propagation by breaking time-reversal symmetry [14–17]. However, the thicknesses of most of the aforementioned designs are nearly as large as the wavelength. It is difficult to design a simple and subwavelength device for acoustic asymmetric transmission because the acoustic wave is not polarized. In this aspect, the single-sided patterned thin

plate based on leaky Lamb and “bending” waves has shown promise for asymmetric transmission because of its relatively simple design, which is amenable to aqueous conditions [18–21]. Analogous designs are difficult to implement for airborne sound because of the large impedance mismatch between air and solid materials. Therefore, it is still a challenge to achieve both simplicity and subwavelength thickness in air.

In this paper, we design a multiband asymmetric transmission device based on an ultrathin coded metasurface formed by an alternating arrangement of the coding elements 0 and 1 [22]. The assembly of the elements is similar to the functional units in a computer system, as it employs a binary system of only two logic levels: 0 for *off* and 1 for *on*. By coding different patterns, such as 0000..., 1111..., and 0101..., the asymmetric transmission effect can be easily controlled to selectively achieve *off* and *on* states. Our strategy is based on the dependence of asymmetric interference on frequencies and incident angles. We can achieve source-free and asymmetric transmission at the subwavelength scale for airborne sound by a simple coding of the metasurface. The proposed metamaterial can be easily fabricated with the existing rapid-prototyping technology. The coded metasurfaces can be used to create flexible acoustic rectifiers because the working frequency is determined solely by the structure factor.

II. DESIGN

Coding elements of 0 and 1 are depicted in Figs. 1(a) and 1(b). Two coding elements are integrated in the form of a smooth and corrugated plate with narrow slits.

*hcheng@nankai.edu.cn

†schen@nankai.edu.cn

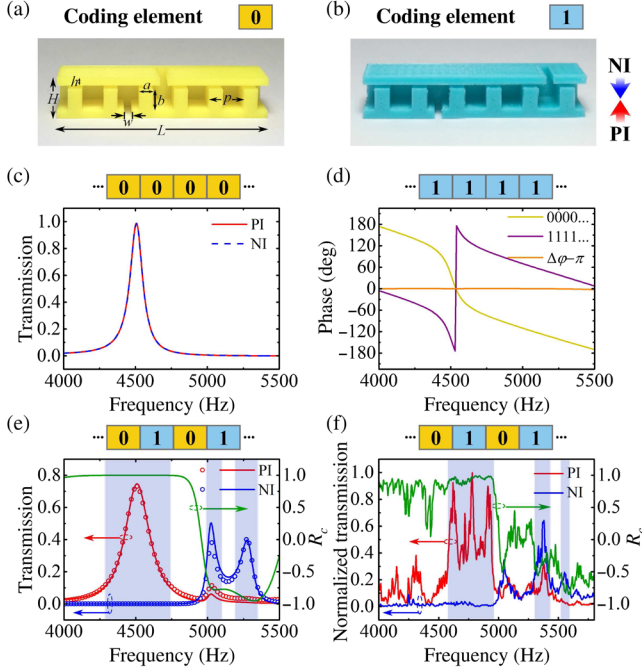


FIG. 1. Schematic diagram of the metasurface coding elements (a) 0 and (b) 1. The pure (c) 0000... or (d) 1111... transmission and phase response for PI and NI. (e) Transmission and contrast ratio of 0101..., with solid lines for simulation data and circles for calculated results. All coding occurs along the x direction. (f) The related experimental result for the transmission and contrast ratio of 0101.... The shaded regions in (e) and (f) represent the simulated and corresponding experimental asymmetric transmission bands.

To maintain generality, we represent the geometric parameters by the element length L . Six rectangular ridges with a width $a = L/15$ and a height $b = L/10$ are equally spaced, with a periodicity $p = L/6$. The narrow slit is located at the $L/3$ position within the corrugated plate of each unit. To break the spatial inversion symmetry, we arrange the slits of the smooth plates at $L/2$ for element 0 and $5L/6$ for element 1. Other geometric parameters are also represented by the element length, such as the total thickness of the element $H = L/5$ (approximately equal to $\lambda/6.3$), the thickness of each plate $h = L/24$, and the width of each narrow slit $w = L/30$. The plate can be considered to be a perfectly rigid body because of the large impedance mismatch with respect to air. Full-wave simulations are performed by the commercial finite-element method (COMSOL Multiphysics), in which the acoustic speed of air is set to $c_0 = 343$ m/s and the density to $\rho_0 = 1.2$ kg/m³.

We define the incidence of an acoustic wave from the corrugated-plate side as positive incidence (PI) and the wave from the smooth-plate side as negative incidence (NI). First, we simulate the transmission of coding patterns 0000..., 1111..., and 0101... for a normal incidence of PI and NI, as shown in Figs. 1(c) and 1(d). The contrast ratio is defined as

$$R_c = \frac{T_{\text{PI}} - T_{\text{NI}}}{T_{\text{PI}} + T_{\text{NI}}}, \quad (1)$$

where T_{PI} and T_{NI} represent the transmission for PI and NI, respectively. The absolute value of R_c indicates the degree of transmission asymmetry, and the sign indicates the directionality of the asymmetric device. The pure coding patterns of 0000... and 1111... produce the same transmission for both PI and NI [see Fig. 1(c)], and the value of R_c is constantly equal to 0, which indicates that no asymmetric phenomenon occurs. There is a phase difference π for the different slit positions between 0000... and 1111..., as shown in Fig. 1(d). When the elements are alternately coded as 0101..., the asymmetric transmission is clearly shown in Fig. 1(e). Thus, the asymmetric transmission effect can be controlled to selectively achieve *off* and *on* by different coding patterns. As shown in Fig. 1(e), there are three asymmetric frequency bands for coding patterns of 0101..., i.e., the first frequency band at approximately 4508 Hz, the second frequency band at approximately 5024 Hz, and the third frequency band at approximately 5274 Hz.

The first asymmetric band is caused by the lower-order resonance, which permits wave transmission from PI. The second and third asymmetric bands are due to the higher-order effect permitting wave transmission from NI. High contrast ratios of $|R_c| > 0.8$ are achieved in the first and third bands, and a contrast ratio of $|R_c| > 0.7$ is achieved in the second band, with blue shaded regions by our design with a subwavelength thickness of approximately $\lambda/6.3$, which is much thinner than previous acoustic designs. The transmission spectrum and the contrast ratio for 3-bit-period and 4-bit-period coding sequences are shown in Figs. S1 and S2 of the Supplemental Material [23]. When 3-bit (001001..., 011011...) and 4-bit (00010001..., 01110111..., 00110011...) sequences and so on are coded, the contributed fields of 0 and 1 may not completely cancel out the transmitted wave for NI, which might diminish the efficiency of the asymmetric transmission. As more propagation modes will occur, more peaks will arise in the transmission spectrum. Additional details may be found in the Supplemental Material [23].

III. EXPERIMENT

The experiment is built in a planar waveguide system in which the sample is firmly sandwiched. The whole waveguide is surrounded by acoustical absorbent material. The sample is composed of seven 1/0 units fabricated by the fused-deposition-modeling 3D-printing technique. A point source is mimicked by guiding the sound from a Brüel & Kjær (B&K) Type 4206 impedance tube through a tiny rubber pipe. The point source is placed 1 m away from the sample. The transmitted wave is scanned with a microphone (B&K Type 4187) to obtain the sound pressure.

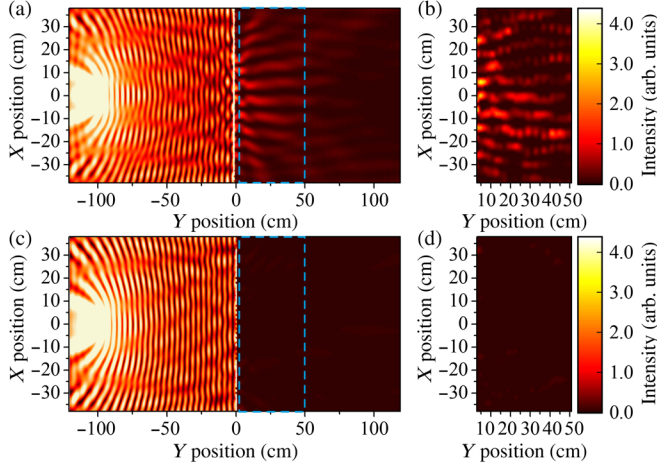


FIG. 2. (a),(c) The simulated and (b),(d) corresponding measured spatial pressure intensity distribution of (a),(b) PI and (c), (d) NI at the first asymmetric band. The measured area is indicated by the blue dashed lines.

The existence of asymmetric transmission is further confirmed by the experiment in Fig. 1(f). Three asymmetric bands can also be found at around 4700, 5380, and 5560 Hz, although the measured transmission efficiency and contrast ratio of the higher asymmetric bands (the second and third bands) are relatively lower than the numerical results. The measured resonant frequencies are blueshifted, which is mainly caused by the deviation in sample fabrication.

To characterize the degree of asymmetry, we show the spatial intensity distribution of the pressure field at the first asymmetric band for both PI and NI. The transmitted wave in the PI case clearly shows a strong pressure intensity distribution as the interference stripes [see Figs. 2(a) and 2(b)], while the transmitted wave in the NI case shows weak pressure intensity [see Figs. 2(c) and 2(d)]. Overall, the experimental result is in great accordance with the simulation, and it shows significant difference between the PI and NI cases.

IV. SIMULATIONS AND DISCUSSIONS

A. Local field

To further investigate the extraordinary phenomenon appearing in the first asymmetric band, the corresponding acoustic pressure distributions are shown in Fig. 3. The local resonances inside the structure of pure 0000... and 1111... are shown in Figs. 3(a) and 3(b). The acoustic pressure distributions are the same for pure 0000... and 1111... for both PI and NI, indicating no asymmetric transmission. It should be noted that the pressure at the input and output slits is in phase for 0000... and out of phase for 1111.... When combining the bits 0 and 1, as shown in Figs. 3(c) and 3(d), the wave of PI is transmitted through constructive interference, whereas the wave of NI

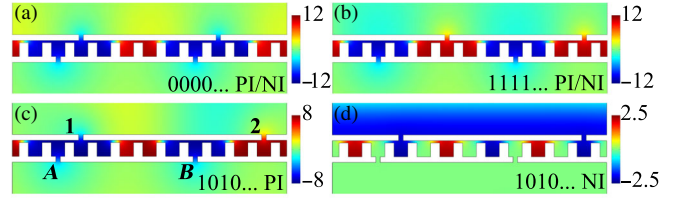


FIG. 3. Simulated pressure distribution (in arbitrary units) in the coding elements (a) 0000... and (b) 1111... for both PI and NI and the simulated pressure distribution in 0101... for (c) PI and (d) NI. The frequency is selected to be the lower-order resonant frequency of 4508 Hz.

is blocked through destructive interference of the local resonance for normal incidence at 4508 Hz. The pressure field exhibits a strong location dependence at the output slits for PI but minimal pressure at the output slits for NI. The asymmetric interference is formed by divergence of the periodic arrangement for the corrugated-plate and quasi-periodic arrangement for the smooth plate, which breaks the space-reciprocal symmetry.

The local resonance is formed by the two-cavity resonant structure. The phase retardation through the two-cavity resonant structure is definitely π because the wave is coupled to the eigenmode corresponding to the point $k_x p / 2\pi = 0.25$ in the first dispersion band. We use slit cavities to couple the wave in or out of the local resonance. Two slit cavities are connected directly for the coding element 0, and they are connected to the left and right ends of a two-cavity resonant structure for the coding element 1. Thus, the phase difference between the coding elements 0 and 1 is π . We define the two slits in the corrugated plate as *A* and *B* and the two slits in the smooth plate as 1 and 2 in Fig. 3(c). For the same reason, the phase difference between the slits of the 0101... structure is $\Delta\varphi_{1,A} = \Delta\varphi_{1,B} = \Delta\varphi_{2,A} + \pi = \Delta\varphi_{2,B} + \pi$.

B. Interference theory

To further investigate the mechanisms of the multiband asymmetric transmission of 0101..., we first simulate the acoustic pressure and relative phase change of the coding unit 01, in which a point source is placed in only one slit (1 or 2) to approximately exclude the influence from the other slit (2 or 1). The pressure field ($p_{n,A}$, $p_{n,B}$) and the relative phase change ($\Delta\varphi_{n,A}$, $\Delta\varphi_{n,B}$) in slits *A* and *B* are probed with the acoustic point source in the slit *n* ($n = 1$ or 2), as shown in Fig. 4. For the lower-order resonance at approximately 4508 Hz, the acoustic contributions from slits 1 and 2 to slits *A* and *B* are equal: $p_{1,A} = p_{2,A} = p_{1,B} = p_{2,B}$. The phase difference is $\Delta\varphi_{1,A(B)} - \Delta\varphi_{2,A(B)} = \pi$. For the NI, the output acoustic fields in slits *A* and *B* are the superposition of the acoustic field transmitted from both slits in the input side, which can be written

$$p_A = Q_1 T_{1,A} e^{i(\phi_1 + \Delta\varphi_{1,A})} + Q_2 T_{2,A} e^{i(\phi_2 + \Delta\varphi_{2,A})}, \quad (2)$$

$$p_B = Q_1 T_{1,B} e^{i(\phi_1 + \Delta\phi_{1,B})} + Q_2 T_{2,B} e^{i(\phi_2 + \Delta\phi_{2,B})}, \quad (3)$$

where Q_1 , Q_2 and ϕ_1 , ϕ_2 are the input acoustic amplitude and phase in slits 1 and 2; $T_{1,A}$, $T_{2,A}$ ($T_{1,B}$, $T_{2,B}$) are the relative transmission from slits 1 and 2 to slit A (B); and $\Delta\phi_{1,A}$, $\Delta\phi_{2,A}$ ($\Delta\phi_{1,B}$, $\Delta\phi_{2,B}$) are the phase changes of the acoustic wave traveling from slits 1 and 2 to slit A (B).

In the same way, for the PI, the output pressure at slits 1 and 2 can also be derived as

$$p_1 = Q_A T_{1,A} e^{i(\phi_1 + \Delta\phi_{1,A})} + Q_B T_{1,B} e^{i(\phi_1 + \Delta\phi_{1,B})}, \quad (4)$$

$$p_2 = Q_A T_{2,A} e^{i(\phi_2 + \Delta\phi_{2,A})} + Q_B T_{2,B} e^{i(\phi_2 + \Delta\phi_{2,B})}. \quad (5)$$

Considering a normally incident plane wave with an amplitude of 1 and an initial phase of 0, along with the periodic arrangement with the same transmission of $T = T_{1,A} = T_{2,A} = T_{1,B} = T_{2,B}$ [see Figs. 4(a) and 4(b)], these equations can be simplified as

$$p_A^{\text{NI}} = T(e^{i\Delta\phi_{1,A}} + e^{i\Delta\phi_{2,A}}), \quad (6)$$

$$p_B^{\text{NI}} = T(e^{i\Delta\phi_{1,B}} + e^{i\Delta\phi_{2,B}}), \quad (7)$$

$$p_1^{\text{PI}} = T(e^{i\Delta\phi_{1,A}} + e^{i\Delta\phi_{1,B}}), \quad (8)$$

$$p_2^{\text{PI}} = T(e^{i\Delta\phi_{2,A}} + e^{i\Delta\phi_{2,B}}), \quad (9)$$

where the superscripts NI and PI denote the incident direction of NI and PI, respectively.

The phase differences for NI induced by the local resonance between the grooves can be written $\Delta\phi_{1,A} = \Delta\phi_{1,B} = \Delta\phi_{2,A} + \pi = \Delta\phi_{2,B} + \pi$, as shown in Fig. 4(c). Thus, we can obtain $p_A^{\text{NI}} = p_B^{\text{NI}} = 0$, resulting in the complete suppression of the transmitted wave. Furthermore, we can obtain $p_1^{\text{PI}} = -2T$ and $p_2^{\text{PI}} = 2T$ in the direction of PI. The constructive interference results in a high transmission amplitude, with the first diffraction

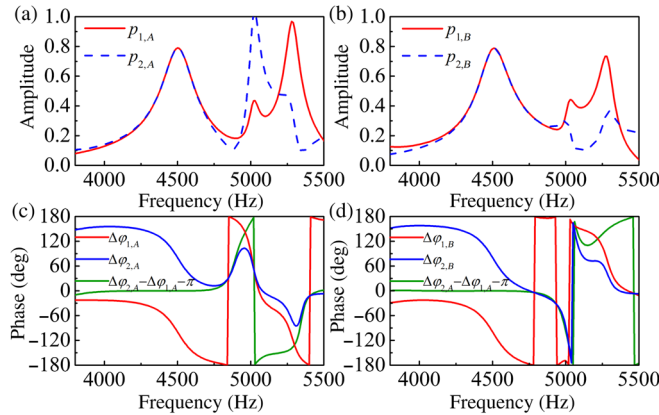


FIG. 4. The pressure amplitude in slits (a) A ($p_{1,A}$, $p_{2,A}$) and (b) B ($p_{1,B}$, $p_{2,B}$) (in arbitrary units), and the relative phase change from slit 1 (or 2) to the slits (c) A ($\Delta\phi_{1,A}$, $\Delta\phi_{2,A}$) and (d) B ($\Delta\phi_{1,B}$, $\Delta\phi_{2,B}$) when a point source is placed in slit 1 (or 2).

order following the generalized Snell's law of refraction, $\sin(\theta_t) = \sin(\theta_i) \pm [\lambda/(2L)]$, where L is the unit length and λ is the wavelength. The broad phase difference of π in Fig. 4(c) gives rise to the broadband phenomena. When combining the two kinds of coding elements, a similar response in terms of the amplitude $T_{1,A} = T_{2,B}$ and phase $\Delta\phi_{1,A} = \Delta\phi_{2,B} + \pi$ from Figs. 1(c) and 1(d) is predictable, but we must be further ensured that it satisfies the amplitude $T_{1,A} = T_{1,B}$, $T_{2,A} = T_{2,B}$ and the phase $\Delta\phi_{1,A} = \Delta\phi_{2,A} + \pi$, $\Delta\phi_{1,B} = \Delta\phi_{2,B} + \pi$. Furthermore, the higher propagation modes result in the higher-order asymmetric transmission bands at approximately 5024 and 5274 Hz, which can be seen from the pressure field in Figs. 4(a) and 4(b), with the corresponding phase shown in Figs. 4(c) and 4(d). The transmission can be further calculated by substituting the results of the pressure and phase in Fig. 4 into Eqs. (2)–(5), as shown by red and blue circles for PI and NI, respectively, in Fig. 1(d). The results are in good agreement with the simulated values, which demonstrates the validity of the theoretical analysis.

C. Angular selectivity

In addition to frequency-selective asymmetric transmission, our designed coding pattern 0101... also exhibits angle-selective transmission. We calculated the transmission as a function of frequency and incident angle for PI and NI in Figs. 5(a) and 5(b), respectively. For the PI, there is only one obvious transmission band (band 1) at approximately 4508 Hz. Band 1 is related to the lower-order resonance, which is sensitive to the incident angle, i.e., within the range of $(-20, 20)$. For the oblique incident wave, the interference patterns will gradually change and eventually exhibit a low transmission rate by changing the phase difference near $2\pi L \sin\theta_i/\lambda$ for the input slits.

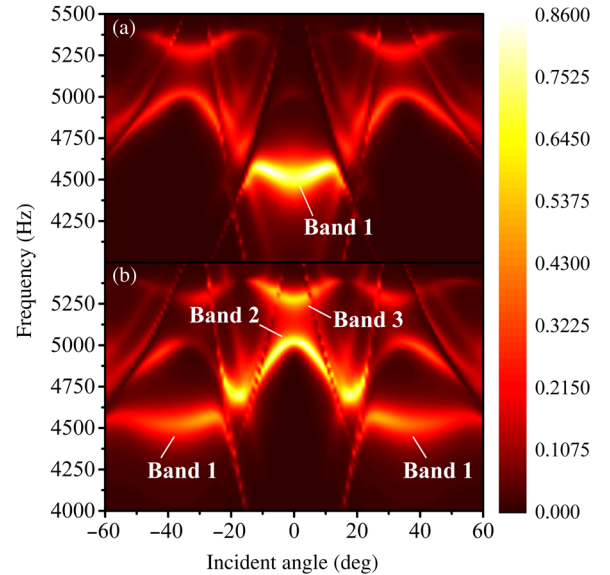


FIG. 5. Simulated acoustic transmission as a function of incident angle and frequency for (a) PI and (b) NI.

However, there are several transmission bands with different frequency and incident angle for NI in Fig. 5(b), i.e., bands 1, 2, and 3. It should be noted that band 1 for NI at approximately 4508 Hz is the reciprocal band of band 1 for PI, with an incident angle consistent with the diffraction angle of band 1 for PI. As the incident angle increases, the transmission for PI rapidly shifts to nearly 0, whereas the transmission for NI shifts from zero to approximately 0.3. The contrast ratio also shifts from 1 to -1 , and the directionality is reversed. By simply rotating the structure, the directionality of the unidirectional transmission can easily be tuned from positive to negative. Higher-order transmission bands of bands 2 and 3 are also found for NI, and both exhibit a good contrast ratio, confirming their suitability for asymmetric transmission design.

V. CONCLUSIONS AND OUTLOOK

In this paper, we theoretically and experimentally investigate an interference-based multiband ultrathin asymmetric device in which angle- and frequency-dependent asymmetric propagation of sound is clearly observed. By breaking the spatial inversion symmetry, constructive interference or destructive interference are coupled for different incident directions and wave bands. Compared to previously proposed acoustic diodes using mode conversion combined with a band-gap material, our ultrathin system offers advantages such as broadband operation, high contrast ratio, and suitability for directional operation. This concept is also expected to inspire other ultrathin unidirectional device designs in both acoustics and photonics.

ACKNOWLEDGMENTS

This work was supported by the National Key Research and Development Program of China (Grant No. 2016YF A0301102), the National Basic Research Program (973 Program) of China (Grant No. 2012CB921900), the Natural Science Foundation of China (Grants No. 11574 163, No. 61378006, and No. 11304163), and the Program for New Century Excellent Talents in University (Grant No. NCET-13-0294).

[1] Z. Liu, X. Zhang, Y. Mao, Y. Y. Zhu, Z. Yang, C. T. Chan, and P. Sheng, Locally resonant sonic materials, *Science* **289**, 1734 (2000).

[2] C. Menzel, C. Helgert, C. Rockstuhl, E.-B. Kley, A. Tünnermann, T. Pertsch, and F. Lederer, Asymmetric Transmission of Linearly Polarized Light at Optical Metamaterials, *Phys. Rev. Lett.* **104**, 253902 (2010).

[3] Y. Cui, L. Kang, S. Lan, S. Rodrigues, and W. Cai, Giant chiral optical response from a twisted-arc metamaterial, *Nano Lett.* **14**, 1021 (2014).

[4] X.-F. Li, X. Ni, L. Feng, M.-H. Lu, C. He, and Y.-F. Chen, Tunable Unidirectional Sound Propagation through a Sonic-Crystal-Based Acoustic Diode, *Phys. Rev. Lett.* **106**, 084301 (2011).

[5] S. Xu, C. Qiu, and Z. Liu, Acoustic transmission through asymmetric grating structures made of cylinders, *J. Appl. Phys.* **111**, 094505 (2012).

[6] Y. Huang, H. Sun, J. Xia, S. Yuan, and X. Ding, Multi-band asymmetric acoustic transmission in a bended waveguide with multiple mechanisms, *Appl. Phys. Lett.* **109**, 013501 (2016).

[7] B. Liang, X. S. Guo, J. Tu, D. Zhang, and J. C. Cheng, An acoustic rectifier, *Nat. Mater.* **9**, 989 (2010).

[8] N. Boechler, G. Theocharis, and C. Daraio, Bifurcation-based acoustic switching and rectification, *Nat. Mater.* **10**, 665 (2011).

[9] T. Devaux, V. Tournat, O. Richoux, and V. Pagneux, Asymmetric Acoustic Propagation of Wave Packets via the Self-Demodulation Effect, *Phys. Rev. Lett.* **115**, 234301 (2015).

[10] T. Biwa, H. Nakamura, and H. Hyodo, Experimental Demonstration of a Thermoacoustic Diode, *Phys. Rev. Applied* **5**, 064012 (2016).

[11] Y. Tanaka, T. Murai, and N. Nishiguchi, Rectification of elastic waves in a thin plate, *J. Appl. Phys.* **111**, 024507 (2012).

[12] Y. Li, B. Liang, Z. Gu, X. Zou, and J. Cheng, Unidirectional acoustic transmission through a prism with near-zero refractive index, *Appl. Phys. Lett.* **103**, 053505 (2013).

[13] C. Shen, Y. Xie, J. Li, S. A. Cummer, and Y. Jing, Asymmetric acoustic transmission through near-zero-index and gradient-index metasurfaces, *Appl. Phys. Lett.* **108**, 223502 (2016).

[14] Z. Yang, F. Gao, X. Shi, X. Lin, Z. Gao, Y. Chong, and B. Zhang, Topological Acoustics, *Phys. Rev. Lett.* **114**, 114301 (2015).

[15] M. Xiao, W.-J. Chen, W.-Y. He, and C. T. Chan, Synthetic gauge flux and Weyl points in acoustic systems, *Nat. Phys.* **11**, 920 (2015).

[16] A. B. Khanikaev, R. Fleury, S. H. Mousavi, and A. Alù, Topologically robust sound propagation in an angular-momentum-biased graphene-like resonator lattice, *Nat. Commun.* **6**, 8260 (2015).

[17] S. H. Mousavi, A. B. Khanikaev, and Z. Wang, Topologically protected elastic waves in phononic metamaterials, *Nat. Commun.* **6**, 8682 (2015).

[18] H. Jia, M. Ke, C. Li, C. Qiu, and Z. Liu, Unidirectional transmission of acoustic waves based on asymmetric excitation of Lamb waves, *Appl. Phys. Lett.* **102**, 153508 (2013).

[19] H. Sun, S. Zhang, and X. Shui, A tunable acoustic diode made by a metal plate with periodical structure, *Appl. Phys. Lett.* **100**, 103507 (2012).

[20] C. Li, M. Ke, Y. Ye, S. Xu, C. Qiu, and Z. Liu, Broadband asymmetric acoustic transmission by a plate with quasi-periodic surface ridges, *Appl. Phys. Lett.* **105**, 023511 (2014).

[21] S. Zhang, Y. Zhang, Y. Guo, Y. Leng, W. Feng, and W. Cao, Realization of Subwavelength Asymmetric Acoustic Transmission Based on Low-Frequency Forbidden Transmission, *Phys. Rev. Applied* **5**, 034006 (2016).

[22] B. Xie, K. Tang, H. Cheng, Z. Liu, S. Chen, and J. Tian, *Adv. Mater.*, DOI: 10.1002/adma.201603507 (2016).

[23] See Supplemental Material at <http://link.aps.org/supplemental/10.1103/PhysRevApplied.7.024010> for details on the transmission spectrum and the contrast ratio for 3-bit-period and 4-bit-period coding sequences.